Supporting Information

Enhancement of Electron Transfer Efficiency in Biofuel Cell Anodes Using Biocompatible Redox-Active Ferritin and Enzyme Assemblies†

Gee Chan Jin[1], Hye Min Yu[1], EuiS Guk Jung[2], Seung-Kyum Choi[3], Yongmin Ko[4]* and Cheong Hoon Kwon[1]*

[1]Department of Energy Resources and Chemical Engineering, Kangwon National University, 346 Jungang-ro, Samcheok, 25913, Republic of Korea

[2]School of Mechanical System Engineering, Kangwon National University, Kangwon-do, 25913, Republic of Korea

[3]George W. Woodruff School of Mechanical Engineering, Georgia Institute of Technology, Atlanta, GA, USA

[4]Division of Energy & Environmental Technology, Material Research Institute, Daegu Gyeongbuk Institute of Science and Technology (DGIST), 333 Techno Jungang-daero, Hyeonpung-eup, Dalseong-gun, Daegu 42988, Republic of Korea

*Address correspondence to yongmin.ko@dgist.ac.kr and chkwon2@kangwon.ac.kr

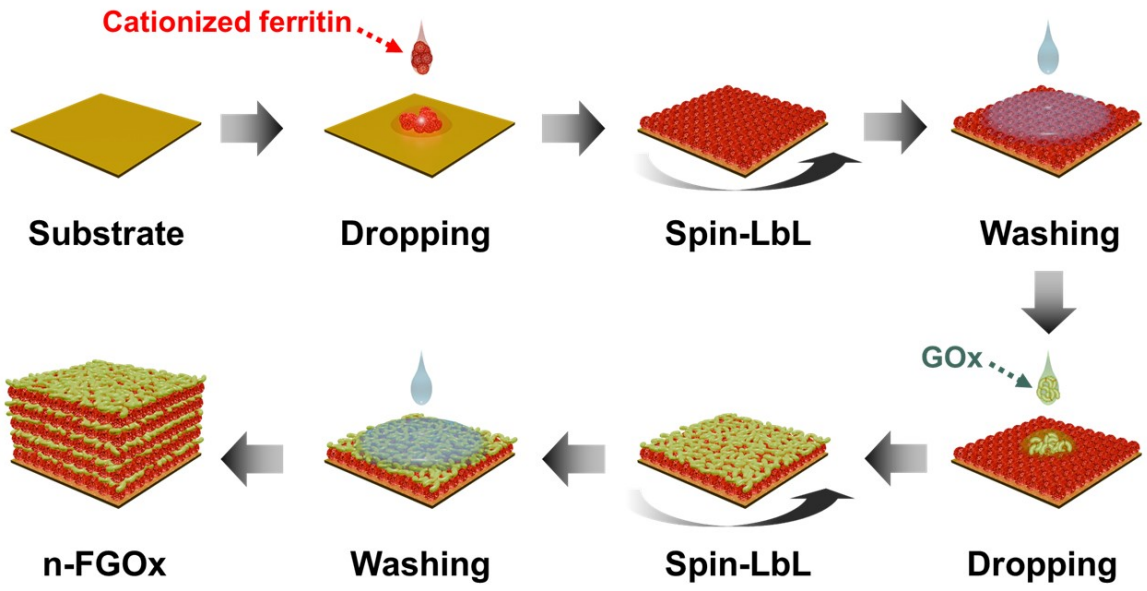

Fig. S1. Schematic representation of the spin coating-assisted LbL assembly process for multilayer film fabrication. The figure illustrates the sequential steps involved in building a multilayer structure using a spin self-assembly technique, which allows precise control of film thickness and composition through alternating deposition and spinning cycles.

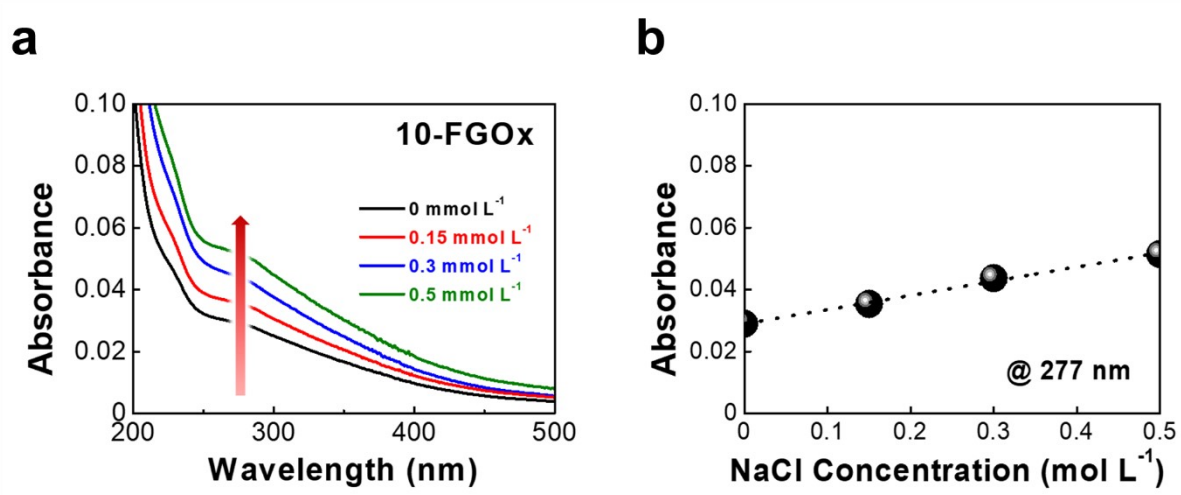

Fig. S2. UV-vis absorbance spectra of 10-FGOx multilayer films prepared with different NaCl concentrations, showing the effect of ionic strength on the assembly and interaction of GOx with cationized ferritin. (a) Absorbance at 277 nm for 1 mg mL^{-1} GOx as a function of NaCl concentration, highlighting a linear trend, reflecting the increased molecular organization and protein density in the multilayer structure with ionic strength. (b) UV-vis spectra for films assembled with 1 mg mL^{-1} GOx, with NaCl concentrations varying from 0 to 0.5 mol L^{-1}, demonstrating a systematic increase in absorbance with higher salt concentrations. The observed shift, particularly at lower wavelengths, indicates enhanced electrostatic interaction between the negatively charged GOx and the positively charged cationized ferritin, promoting stronger binding and denser film formation.

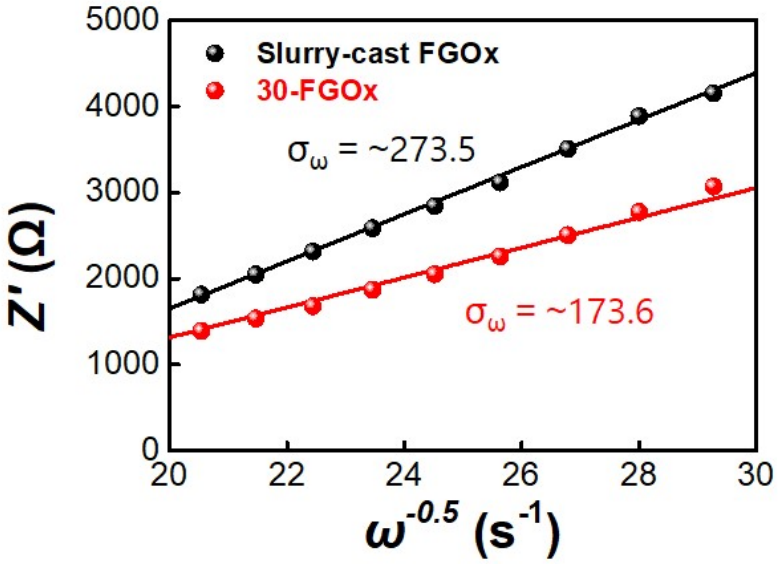

Fig. S3. Warburg impedance of 30-FGOx and slurry-cast FGOx electrodes. The Plots was calculated under 300 mmol L^{-1} glucose concentration. The Warburg impedance spectra slope indicates that 30-FGOx has smoother charge transfer than slurry-cast FGOx.

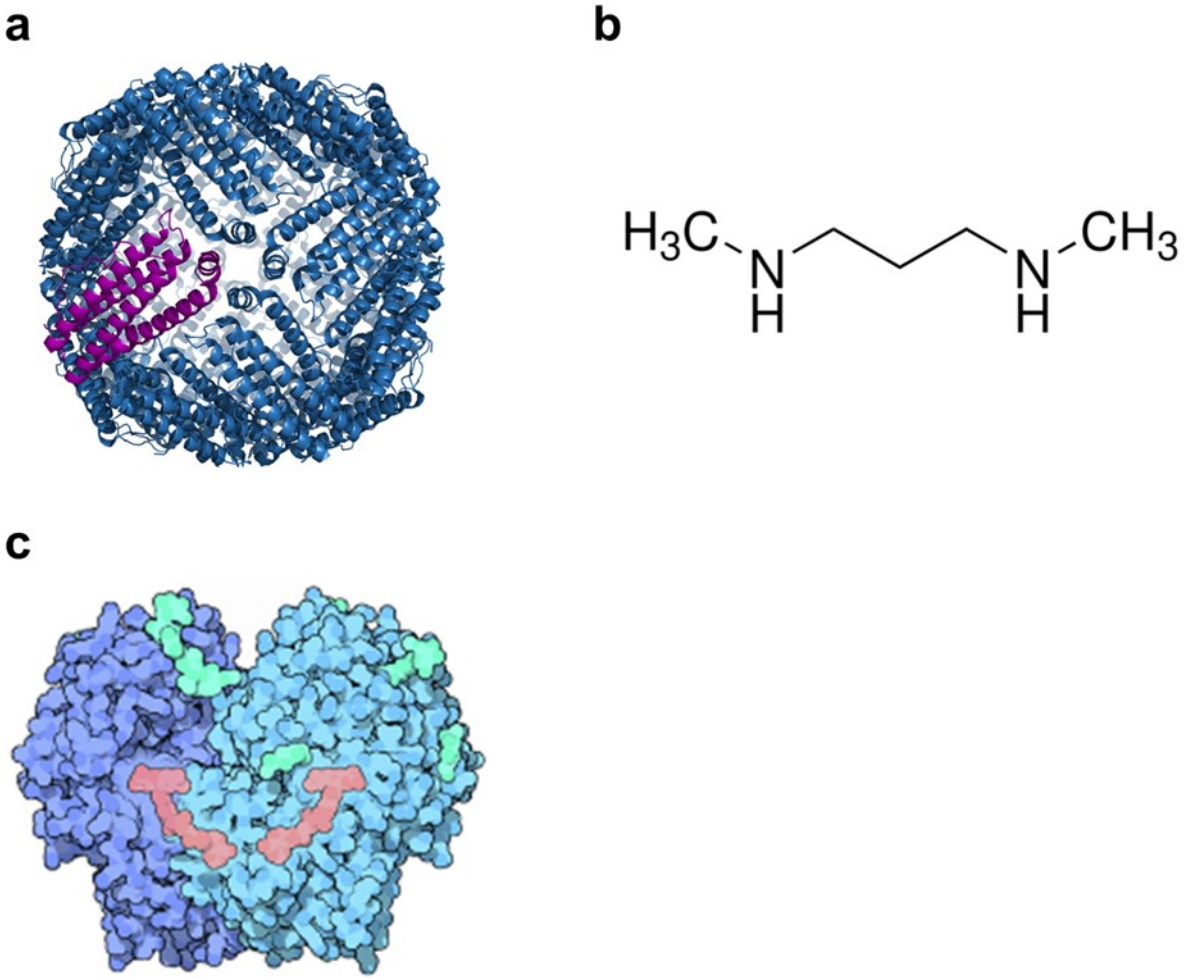

Fig. S4. Chemical structures related to the components used in the functionalization of cationized ferritin and the structure of GOx. (a) Ferritin, a protein that stores iron in the body and releases it in a controlled manner. It is found primarily in the liver, spleen, bone marrow, and muscles. (b) N,N-dimethyl-1,3-propanediamine (DMPA), a derivative of naphthalene used as a stabilizing or hydrophobic moiety in some biological applications. This structure shows its tertiary amine functionality attached to the naphthalene ring, which enhances hydrophobic interactions. (c) GOx, a polymeric enzyme consisting of glucose-binding regions, shown here as a polysaccharide structure, which catalyzes the oxidation of glucose to gluconic acid, an important reaction in biosensor applications.

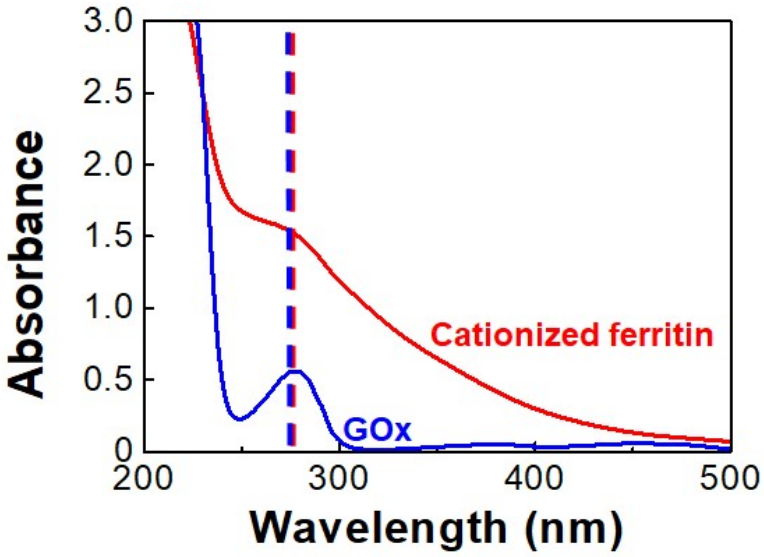

Fig. S5. UV-vis absorption spectra comparing cationized ferritin and GOx and their multilayer assembly. The UV-vis spectra of cationized ferritin (red line) show a prominent absorption peak at 280 nm, characteristic of aromatic protein residues such as tyrosine and tryptophan. In contrast, the GOx spectrum (blue line) shows a peak at 277 nm, corresponding to the intrinsic absorption of the protein, which is mainly influenced by its flavin adenine dinucleotide (FAD) cofactor and aromatic amino acids.

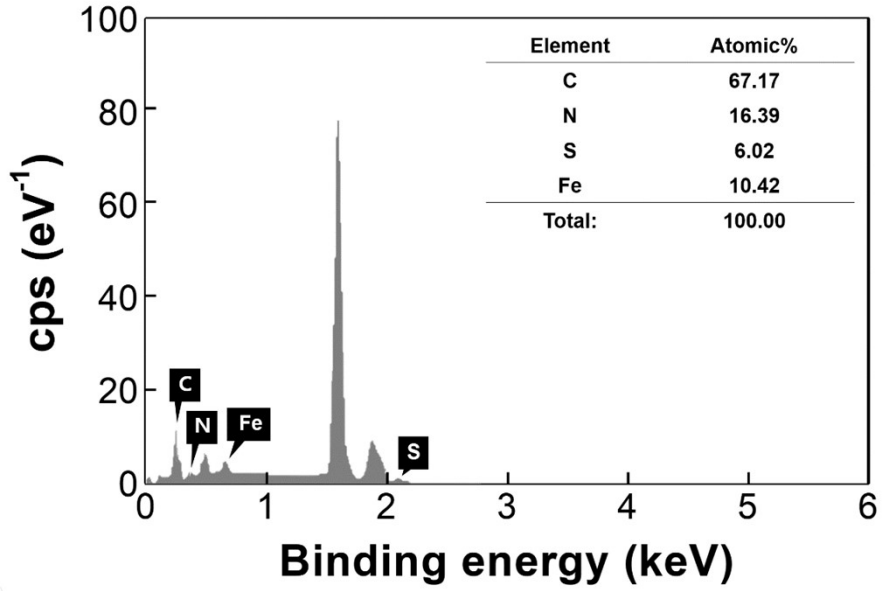

Fig. S6. Energy-dispersive X-ray spectroscopy (EDS) analysis of 30-FGOx multilayers, showing the presence of sulfur (S) from the enzyme and iron (Fe) from ferritin. The atomic percentage composition includes carbon (C), nitrogen (N), sulfur (S), and iron (Fe), confirming the successful integration of enzyme and ferritin in the multilayer structure.

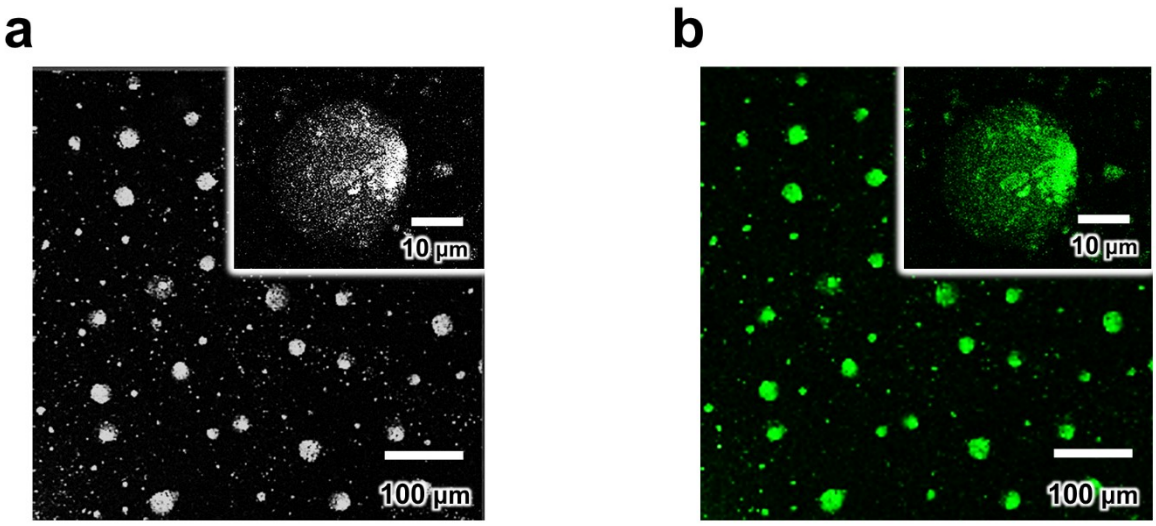

Fig. S7. Confocal microscopy images of the (ferritin/GOx)$_3$ multilayer assembly. (a) Confocal transmission image highlighting the distribution of the assembly, with the inset showing a magnified view of the structural features. (b) Confocal fluorescence image of fluorescein isothiocyanate (FITC)-labeled GOx within the multilayer assembly, with the inset providing a detailed close-up of the fluorescence signal.

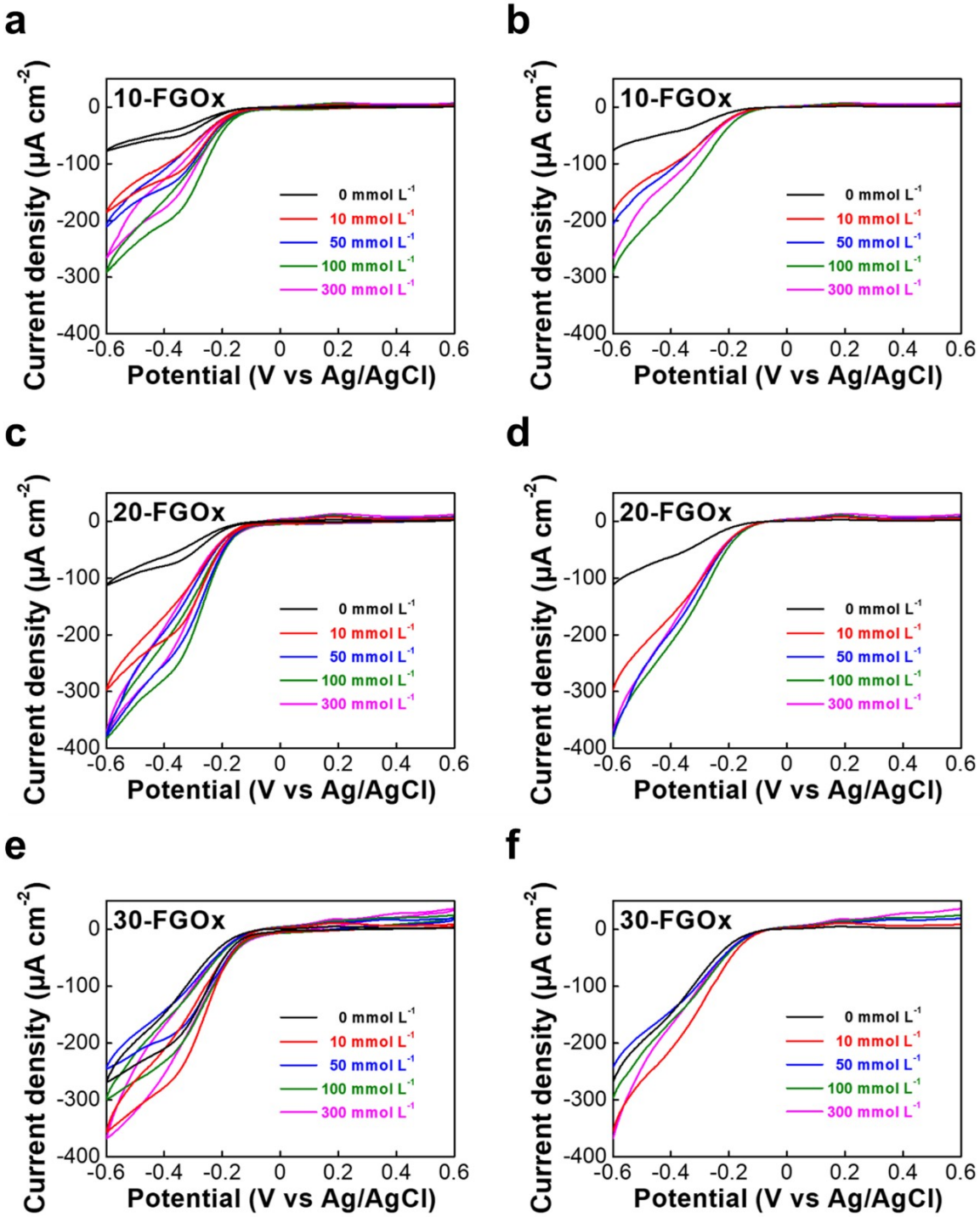

Fig. S8. CVs for the multilayer system of n-FGOx at different glucose concentrations. This figure displays the cyclic voltammetry profiles for multilayered cationized ferritin and glucose oxidase assemblies at varying layers (n = 10, 20, and 30) under different glucose concentrations (0, 10, 50, 100, and 300 mmol L^{-1}). (a, c, e) CVs for n-FGOx showing the typical redox

behavior, where glucose oxidation leads to increasing current densities at higher glucose concentrations. (b, d, f) Oxidation current density for n-FGOx. As the glucose concentration increases, the oxidation peak current shows a more pronounced increase, reflecting the enhanced catalytic activity of the multilayer structure.

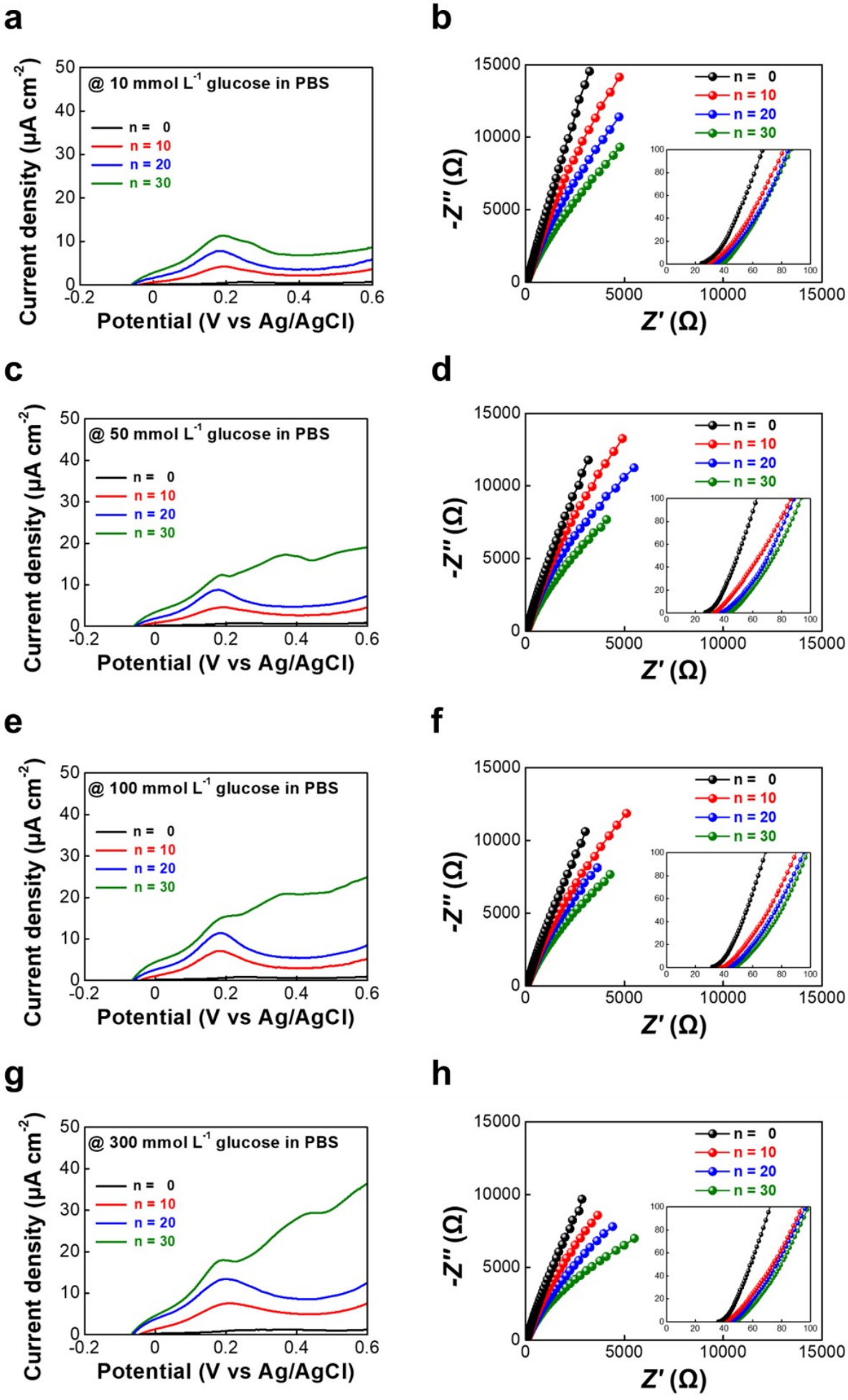
a
@ 10 mmol L-1 glucose in PBS
n = 0
n = 10
n = 20
n = 30
Current density (μA cm-2)
Potential (V vs Ag/AgCl)
b
-Z'' (Ω)
Z' (Ω)
c
@ 50 mmol L-1 glucose in PBS
d
e
@ 100 mmol L-1 glucose in PBS
f
g
@ 300 mmol L-1 glucose in PBS
h

Fig. S9. Cyclic voltammograms (CVs) and Nyquist plots for n-FGOx multilayers (n = 0, 10, 20, 30) at different glucose concentrations (10, 50, 100, and 300 mmol L^{-1}) in PBS. (a, b) under 10 mmol L^{-1} glucose, (c, d) under 50 mmol L^{-1} glucose, (e, f) under 100 mmol L^{-1} glucose. (g, h) under 300 mmol L^{-1} glucose.

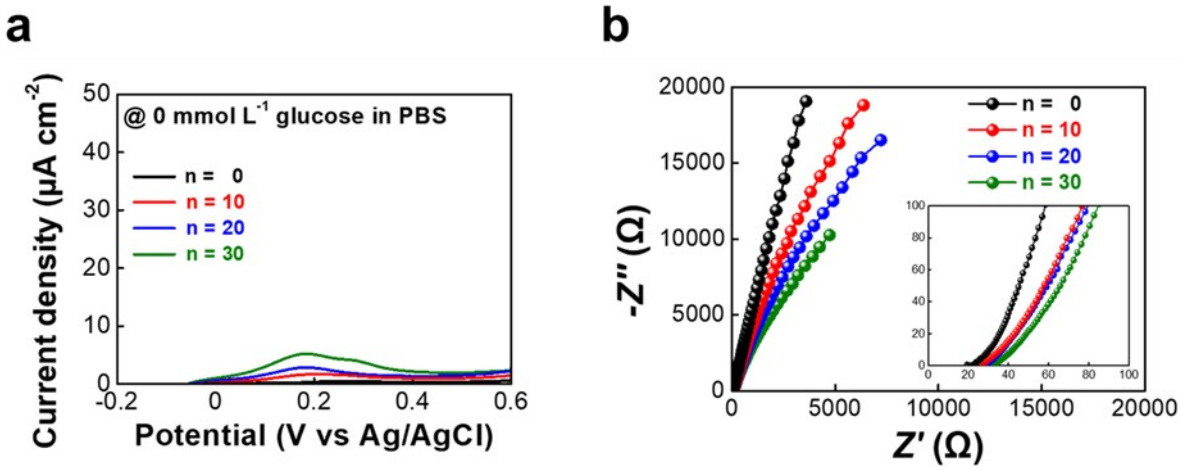

Fig. S10. CVs and EIS Nyquist plots for n-FGOx multilayers (n = 0, 10, 20, 30) under glucose-free conditions. (a) Oxidation current density from CVs at 0 mmol L^{-1} glucose in PBS. (b) Nyquist plot from EIS measurements. Inset shows the low-frequency region.

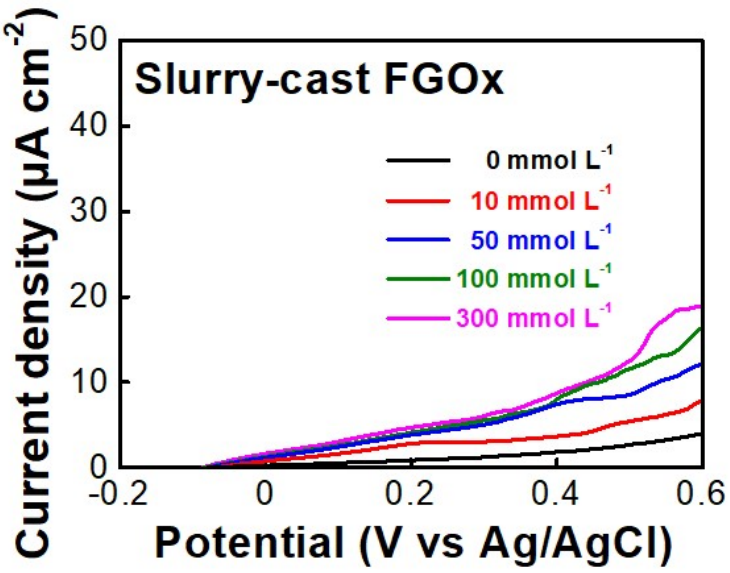

Fig. S11. CVs for slurry-cast anode composed of cationized ferritin and GOx at different glucose concentrations (i.e., 0, 10, 50, 100, and 300 mmol L^{-1}).

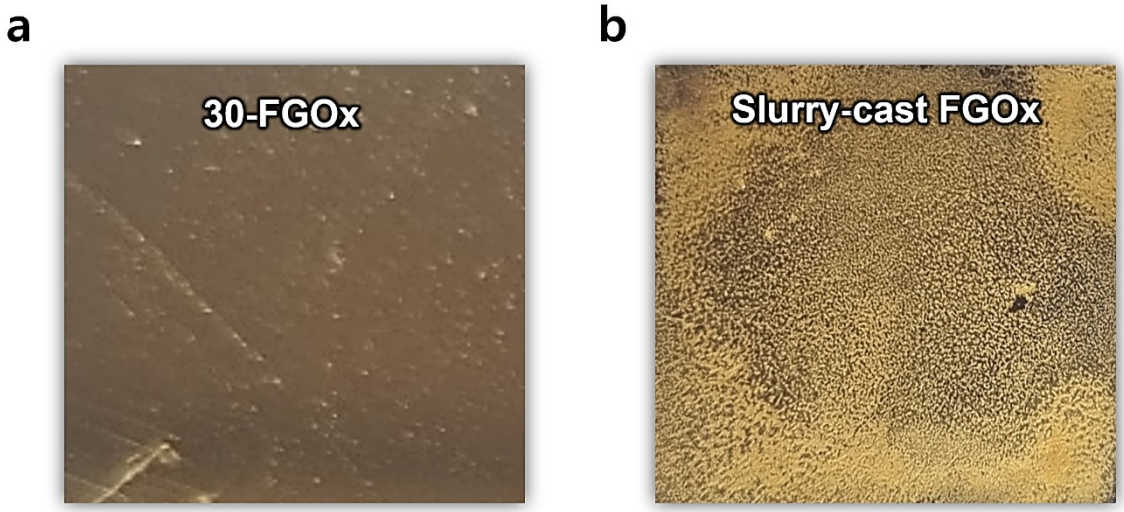

Fig. S12. Comparative visual representation of the FGOx anodes fabricated via different methods. (a) 30-FGOx anode. (b) Slurry-cast FGOx anode.

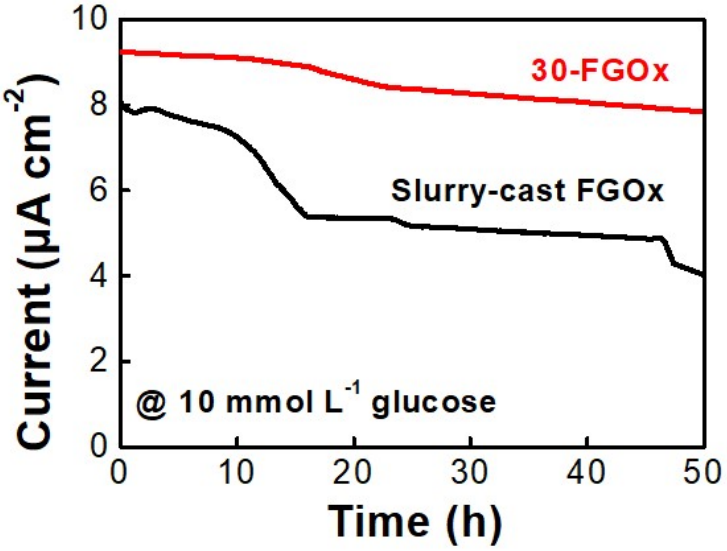

Fig. S13. Long-term stability for 30-FGOx and slurry-cast FGOx electrodes at 10 mmol L^{-1} glucose concentration. The 30-FGOx electrode (red curve) shows a relatively stable current density, maintaining a higher value over 50 h compared to the slurry-cast FGOx electrode (black curve). The slurry-cast FGOx exhibits a more pronounced current decay, indicating a loss of activity.